J. Synchrotron Rad. (2000). **7**, 340–347

Fixed-exit monochromator for computed tomography with synchrotron radiation at energies 18–90 keV

P. Suortti,[a]*† S. Fiedler,[a] A. Bravin,[a] T. Brochard,[a] M. Mattenet,[a] M. Renier,[a] P. Spanne,[a]‡ W. Thomlinson,[a] A. M. Charvet,[b] H. Elleaume,[b] C. Schulze-Briese[c] and A. C. Thompson[d]

[a]European Synchrotron Radiation Facility, BP 220, F-38043 Grenoble, France, [b]Unite IRM, CHU, BP 217, F-38043, Grenoble, France, [c]Swiss Light Source, CH-5232 Villigen PSI, Switzerland, and [d]Center of X-ray Optics, Lawrence Berkeley Laboratory, Berkeley, CA 94720, USA. E-mail: pekka.suortti@helsinki.fi

(*Received 10 March 2000; accepted 12 June 2000*)

A fixed-exit monochromator has been constructed for computed tomography (CT) studies at the Medical Beamline of the European Synchrotron Radiation Facility. A non-dispersive pair of bent Laue-type crystals is used, and the first crystal is water-cooled. The monochromator operates at energies from 18 to 90 keV, and the maximum width of the beam is 150 mm. The performance of the monochromator is studied with respect to the beam intensity and energy distributions, and a close agreement is found between the calculated and experimental results. The intensity is between 10^9 and 10^{10} photons s^{-1} mm^{-2} under typical operating conditions. The harmonic content of a 25 keV beam is about 30% at the minimum wiggler gap of 25 mm (field 1.57 T) and decreases by an order of magnitude when the gap is increased to 60 mm (field 0.62 T). The experimental set-up for CT studies includes dose monitors, goniometers and translation stages for positioning and scanning the object, and a 432-element linear-array Ge detector. Examples from phantom studies and *in vivo* animal experiments are shown to illustrate the spatial resolution and contrast of the reconstructed images.

Keywords: X-ray optics; monochromators; computed tomography; X-ray imaging.

1. Introduction

The synchrotron radiation fan from a wiggler source is several mrad wide, while the height is only 0.1 mrad. Such a beam is ideally suited for computed tomography provided that the distance to the source is large. The spectral flux is very high, typically 10^{14} photons s^{-1} mrad $(hor)^{-1}$ (0.1% bandwidth)$^{-1}$, so that sufficient intensity at the patient can be achieved even when a narrow energy band is extracted by a crystal monochromator. The use of monochromatic synchrotron radiation has several advantages in computed tomography (CT). First, beam hardening is eliminated or strongly reduced if the monochromator rejects most of the harmonic energies. Second, the energy can be tuned to either side of the absorption edge of the contrast agent, so that the distribution of very diluted contrast agent is seen in a subtraction image of thick strongly absorbing tissues. Third, the available energy range is wide, so that the contributions of different elements to absorption can be selectively enhanced or suppressed. Fourth, the natural collimation of the beam allows for large distances between the patient and the detector, so that blurring of the image due to scattering is eliminated, and efficient one-dimensional detectors can be used.

The concept of CT with synchrotron radiation was introduced 15 years ago (Thompson *et al.*, 1984) and in recent years experiments have been started in several laboratories (Graeff & Engelke, 1991; Dilmanian, 1992; Nagata *et al.*, 1992; Elleaume *et al.*, 1997). On the experimental side, one of the main issues has been the development of monochromators that provide a wide, homogeneous and stable beam of easily tunable energy in the range 20–100 keV. Problems arise from the facts that the monochromator crystal is subjected to a high heat load, and in a fixed-exit double-crystal monochromator the reflection angles must be maintained to a fraction of the width of the reflectivity curve. This width is only a few μrad for perfect flat crystals at high X-ray energies, and the condition of non-dispersive setting must be met for a beam that is 15 cm or even 30 cm wide. Many attempts at constructing such monochromators using flat crystals have failed. The basic difficulty of the very narrow reflectivity curves can be solved by the use of bent crystals in transmission (Laue) geometry. The width of the reflectivity curve can be regulated by the bending radius, thickness and asymmetry angle of the crystal. At the same time, different focusing geometries can be realized (Suortti *et al.*, 1997).

† Present address: Department of Physics, PO Box 9, FIN-00014 University of Helsinki, Finland.
‡ Deceased.

The use of bent crystals as X-ray optical elements has become a well established practice in the last few years, and different constructions for a great variety of applications have been put forward. In particular, focusing Laue monochromators have made possible routine studies of intravenous coronary angiography with synchrotron radiation (Suortti *et al.*, 1993; Illing *et al.*, 1995), and this success encouraged us to apply the same ideas in the X-ray optics for CT. Actually, the basic concept of the present design was presented more than five years ago by some of the present authors (Schulze *et al.*, 1994).

2. Reflection by bent crystals

Focusing by a bent crystal follows the principles familiar from light optics. There is an important difference, however. The direction of the ray reflected from a crystal is determined by the orientation of the Bragg planes, which make an angle χ with the normal of the crystal surface. There is specular reflection of a narrow energy band from the Bragg planes and, when the ray penetrates into a bent crystal, this band shifts, the direction of the reflected ray changes, and there is a lateral displacement of the reflected ray. For a complete description of diffraction by a bent crystal the trajectories of the incident and reflected rays inside the crystal must be calculated and then integrated over the incident beam and the active volume of the crystal in the position-angle space. In the idealized case of a thin crystal, geometrical focusing can be treated separately from the trajectory of an individual ray.

Focusing by an ideal cylindrically bent thin crystal is shown in Fig. 1 for the Laue case. It should be noted that the propagation direction can be inverted in the figures. There are several special cases, *e.g.* when the source is on the focusing (Rowland) circle a monochromatic beam of the original divergence is reflected, or when the source is at the mid-point of the chord inside the Rowland circle a parallel polychromatic beam is reflected, or radiation from a source outside the Rowland circle is reflected to a polychromatic focus inside the circle. The focal distances p (source-to-crystal) and q (crystal-to-image) are related through

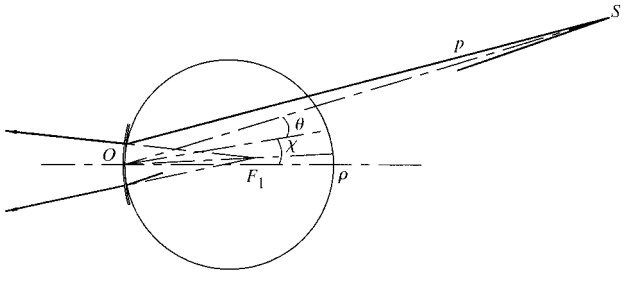

Figure 1
Reflection from a cylindrically bent Laue crystal. The source S is at distance p from the crystal center O, ρ indicates the bending axis, χ the asymmetry angle, and θ the Bragg angle of reflection. The focus is at F_1.

$$q = q_o/(2 - p_o/p), \tag{1}$$

where

$$p_o = \rho\gamma_o = \rho\cos(\chi + \theta),$$
$$q_o = \rho\chi_h = \rho\cos(\chi - \theta)$$

are the focal distances for monochromatic focusing (Suortti *et al.*, 1997). Here, θ is the Bragg angle, χ is the angle between the Bragg planes and the surface normal of the crystal, ρ is the bending radius, and γ_o and γ_h are the direction cosines of the incident and reflected beams, respectively. A band of energies, ΔE, is reflected due to the equatorial divergence of the incident beam, $\Delta\psi = h/p$, unless the source is on the Rowland circle. The relative width of this band is

$$\Delta E/E = \cot\theta\, h(1/p_o - 1/p). \tag{2}$$

The FWHM of the reflectivity curve of a sufficiently thick weakly absorbing perfect crystal in Laue geometry is the so-called Darwin width, which corresponds to a relative energy band

$$(\delta E/E)_{\rm D} = M^{1/2}(4\, r_e\, d^2/\pi V_c)CF'. \tag{3}$$

Here, $M = \gamma_h/\gamma_o$ is the magnification factor, $r_e = e^2/mc^2$ is the classical electron radius, d is the spacing of lattice planes, V_c is the volume of the unit cell, C is the polarization factor (= 1 for σ polarization and $\cos 2\theta$ for π polarization), and F' is the real part of the structure factor. The relative bandwidth is independent of energy except in the vicinity of the absorption edges. In the case of low-order reflections of Si, the relative bandwidth is about 10^{-4} and decreases rapidly for higher-order reflections.

When a crystal of thickness T is bent cylindrically to the radius ρ, the width of the reflectivity curve is given by

$$\delta\theta_{\rm B} = (T\tan\chi/\rho\cos^2\theta)(\gamma_h/\gamma_o)^{1/2} \times\{1 + [(\cos 2\theta + \cos 2\chi)/2] \times[1 - (s_{13} + s_{15}\cot\chi)/s_{11}]\}, \tag{4}$$

where s_{ij} are the elastic compliances for a given crystal orientation and asymmetry angle (Schulze *et al.*, 1998). The reflectivity curve can be calculated using the geometrical theory of diffraction from a deformed crystal (Penning & Polder, 1961; Kato, 1964; Schulze & Chapman, 1995). Experiments have validated the theoretical results and demonstrated that the energy bandwidth $(\delta E/E)_{\rm B}$ may be one or even two orders of magnitude larger than $(\delta E/E)_{\rm D}$ (Schulze *et al.*, 1994). The bandwidth and focusing conditions can be tailored to the needs of the experiment by proper choices of the thickness, asymmetric cut and bending radius of the crystal.

3. Bent Laue–Laue monochromator

In CT imaging, rather wide energy bands are adequate, *e.g.* from 0.1% to 1%. These can be achieved with bent Laue crystals, and it is evident that two crystals with wide reflectivity curves can be matched much more easily than

two flat crystals. Various two-crystal combinations have been considered previously (Suortti *et al.*, 1997), and these differ with respect to focusing properties and energy bandpass. The non-dispersive setting of the two crystals can be realized in many ways, and the present choice is shown in Fig. 2(*a*). The source is on the concave side of the crystals, which means that the bending radius ρ in equation (1) is positive, as well as p_o and p. Monochromatic beam is obtained when the source is on the Rowland circle, but it can be seen from equation (2) that the crystals can be overbent to increase the width of the reflectivity curve without an undue increase of the total bandwidth. In the non-dispersive setting the virtual focus of the first crystal is the source for the second crystal, and a fixed-exit tunable beam is obtained when the distance between the crystals is adjusted appropriately. The antisymmetric setting of the crystals makes the beam paths inside the crystals equal [the case of 'upper signs' for both crystals (Suortti & Thomlinson, 1988)], and it eliminates off-equatorial reflections. The bending radii of the crystals are not equal, but in this 'upper–upper' case

$$\rho_2 = [\rho_1 \cos(\chi - \theta) + L]/\cos(\chi + \theta), \qquad (5)$$

where L is the distance between the crystals. The transmitted energy band is that given by (2) and convoluted by the combined reflectivity curve $R(\theta)$ of the two crystals. The matching condition for the two crystals requires that the energy band reflected by the first crystal from any given polychromatic ray is reflected by the second crystal. The energy, propagation direction and position are correlated in this band, as sketched in Fig. 2(*b*). A simple geometrical reasoning suggests that the thickness of the second crystal, T_2, should be twice that of the first crystal, *i.e.* $T_2 = 2T_1$, in order to span the required energy band. However, the actual matching conditions are rather complex, and detailed calculations would be needed for each situation (Schulze *et al.*, 1998). The present work focuses on the practical aspects of the monochromator construction, and identical crystals are used. The matching conditions for geometrical focusing and energy bands can be summarized by the requirement that the individual reflectivity curves $R_1(\theta)$ and $R_2(\theta)$ should coincide over the entire cross section of the beam. Deviations from this condition cause losses and inhomogeneity of intensity and energy distributions of the exit beam, as discussed later.

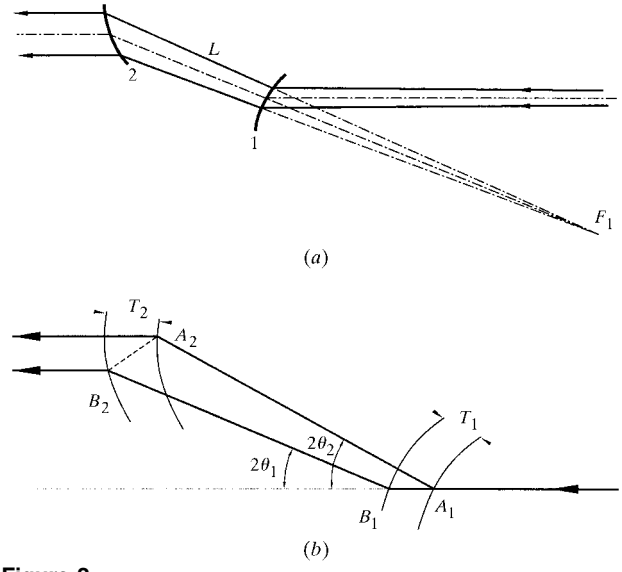

Figure 2
Geometrical and energy-band matching of reflections in two bent Laue crystals. The geometrical condition for the 'upper–upper' case ($\theta > 0$ for both crystals) is shown in (*a*): the focal line F_1 of the first crystal is the source for the second crystal. Matching of the energy bands is shown in (*b*): the Bragg angle changes between A_2 and B_2 by an amount that corresponds to the changes of energy and propagation direction between A_1 and B_1.

The properties and performance of the bent-crystal Laue–Laue monochromator have been studied recently in detail (Ren *et al.*, 1999). Compared with a flat-crystal Laue–Laue monochromator, the bent-crystal monochromator provided a much improved beam stability, about tenfold increase in flux, and a large reduction of harmonic contamination. The bent-crystal monochromator was not cooled, so that the beam power had to be reduced by absorbers. For the actual beamline operations the flux is

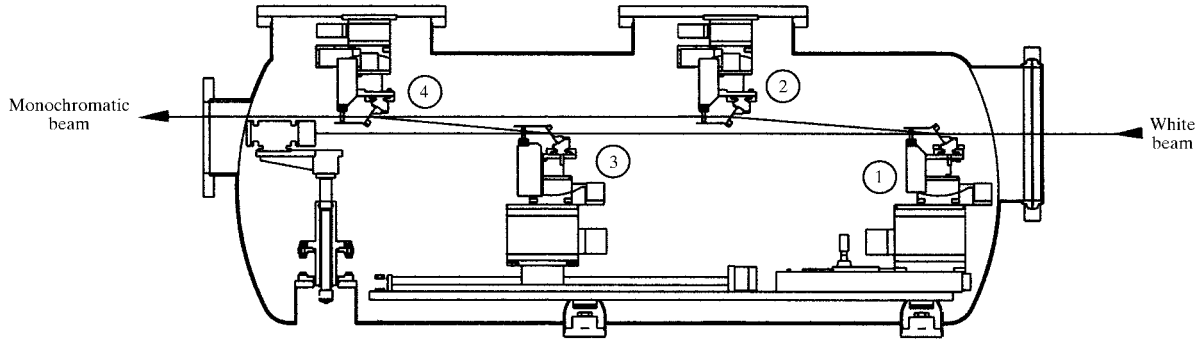

Figure 3
Layout of the monochromators at the Medical Beamline ID17 of the ESRF. Two pairs of CT monochromators can be installed in the tank; at the moment only the pair in positions 3 and 4 are in use. The crystals can be tilted about horizontal axes, and the first crystal can be translated vertically and along the beam direction. The vertical offset of the beam is 40 mm. The first crystal and the beamstop can be lowered to allow the use of the dual-energy monochromator for coronary angiography, located downstream in another tank.

usually maximized, and the spatial constraints determine the distances between the source, monochromator, object and the detector. The construction of the monochromator is a compromise where the parameters are chosen to match these conditions and, at the same time, the problems arising from the heat load and mechanical instabilities must be solved. It is important that the use of bent crystals leaves much flexibility for optimization of the design. In this paper we describe a monochromator which was constructed for routine use at the Medical Beamline of the ESRF.

The monochromator is located in a special hutch of the Medical Beamline (ID17) at the ESRF. The general layout of the beamline has been described recently (Elleaume *et al.*, 1999). The construction of the CT monochromator is shown in Fig. 3. There are two pairs of crystals for a rapid change of energy by a beam selector, but at the moment only one pair has been installed at positions 3 and 4. The first crystal is placed on a precision stage for tilts and vertical translation, and it can be translated along the beam direction to provide a fixed exit beam with 40 mm offset in the energy range 18–90 keV. The monochromator crystals are 150 mm wide, and the incident beam is limited by vertical and horizontal slits in front of the monochromator. The monochromator crystal and cooling system are shown in Fig. 4. The upper and lower parts of the crystal are thick in order to provide stiffness and good thermal contact to the cooling tubes, and the 20 mm-high center part is about 1 mm thick. The crystal is clamped by the base, and leaf springs are attached to the upper part. When the free ends of the springs are pushed, the thin center part of the crystal curves to a cylindrical shape due to the bending moment introduced by the springs. The travel of the actuators bending the springs is large, typically about 10 mm, which is important for stability against thermal drifts and vibrations of the mechanical structures.

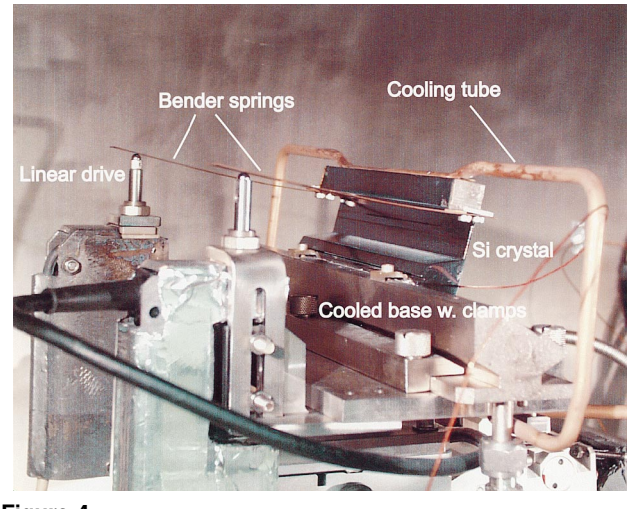

Figure 4
Photograph showing the cross section, cooling and bending mechanisms of the first crystal. The tube for water cooling is in contact with InGa eutectic in the groove in the top part of the crystal.

Under typical conditions the first crystal is exposed to a beam where the maximum power density is 1–2 W mm^{-2}, and the total absorbed heat load to be transferred by cooling is of the order of 50 W for a 1 mm-high beam. The base of the crystal is clamped to a water-cooled Cu block, and there is a thin layer of InGa eutectic between the crystal and the cooling block. The upper part of the crystal has an 8 mm-wide groove, which is partly filled with InGa. A water pipe is partly immersed in the eutectic without making contact with the crystal itself. It is important that the cooling and bending are separated, so that the only forces acting on the crystal are those transmitted by the springs and the clamps of the base. This construction was first introduced for the angiography monochromator at the NSLS in Brookhaven (Thomlinson, 1996). The second crystal is identical to the first one, but it is not cooled. However, the beamstop is rather close to the crystal, and a collar was installed in front of the beamstop to prevent heating of the crystal by scattered radiation. When the other pair of crystals at positions 1 and 2 are used, a beam selector, which chooses the beams from the first or second pair of crystals, is placed close to the second crystal of the downstream pair. The first crystals of each pair reflect bands of pre-set energies towards the respective second crystals, and the energy is selected by blocking one of the beams either after or before the second crystal. In this way the heat loads on the first crystals are kept constant, which is essential for thermal stability.

4. Flux and harmonics

The brightness of the X-ray beam on the sample can be calculated from the source parameters, attenuation in the beamline windows and filters, and the reflectivity of the monochromator crystals. Most experimental tests were made at 25 and 33 keV, which are the relevant energies for mammography and *K*-edge subtraction imaging with iodine as the contrast agent. At these energies the central spectral brightness of the X-ray beam from the 21-pole permanent magnet at a gap of 25 mm is calculated to be about 1.3×10^{15} photons s^{-1} mrad^{-2} (100 mA)$^{-1}$ (0.1% bandwidth)$^{-1}$. Calculated reflectivity curves $R_1(\theta) = R_2(\theta)$ of a monochromator crystal are shown in Fig. 5. It was discussed earlier that probably 50% of the energy band from the first crystal is reflected by the second one, so that when the crystals are perfectly aligned the integrated reflectivity of the pair is $(1/2)\int[R_1(\theta)]^2\,\mathrm{d}\theta$. In the case of a two-dimensional beam it is required for a perfect alignment that the bending radii of the crystals fulfill the condition given above and that the axes are parallel and horizontal. Any deviation from these conditions will shift the reflectivity curves R_1 and R_2 with respect to each other with a subsequent loss of intensity.

In the present case the bending radii of the Si(111) crystals, 30 m, are rather large, the thickness of the crystals is 1.2 mm, and the asymmetry angle $\chi = 15°$. The width of the reflectivity curve in the energy scale, as calculated from

equation (4), is 4×10^{-4}, *i.e.* three times the Darwin width. The central brightness of the monochromatic beam is

$$(\mathrm{d}^2 n_{o,m}/\mathrm{d}\theta \mathrm{d}\psi)_o = (\mathrm{d}^2 n_o/\mathrm{d}\theta \mathrm{d}\psi)_o \cot\theta \int R(\theta)\,\mathrm{d}\theta, \quad (6)$$

where the central brightness of the incident beam n_o is that for 100% bandwidth. For the measurement of the brightness a small beam [1 mm (V) × 2 mm (H)] was used, and the monochromator was tuned for maximum flux, *i.e.* for the maximum overlap of R_1 and R_2 at the beam center. The monochromatic flux was measured by Compton scattering from an Al plate of known thickness. The observed scattered flux is

$$n_\mathrm{C} = n_{o,m} M_\mathrm{el} (\mathrm{d}\sigma/\mathrm{d}\Omega)_\mathrm{KN} \Omega t A, \quad (7)$$

where $n_{o,m}$ is the incident monochromatic flux, M_el is the number of electrons in unit volume, $(\mathrm{d}\sigma/\mathrm{d}\Omega)_\mathrm{KN}$ is the Klein–Nishina scattering cross section for one electron, Ω is the solid angle subtended by the detector, t is the thickness of the sample, and A is the absorption factor. The Klein–Nishina cross section is given by

$$(\mathrm{d}\sigma/\mathrm{d}\Omega)_\mathrm{KN} = r_e^2 k_\mathrm{pol}/[1 + (E/mc^2)(1 - \cos\Theta)]^2, \quad (8)$$

where Θ is the scattering angle, and the polarization factor $k_\mathrm{pol} = \cos^2\Theta = 0.75$ in the present case of linearly polarized radiation and a scattering angle in the horizontal plane of 150°. Calculated and measured values of the central brightness of the monochromatic beam are collected in Table 1. The reflectivity of the monochromator was calculated using the *PEPO* code (Schulze & Chapman, 1995), and perfect matching of the crystals was assumed in the small beam area. The attenuation factor is due to carbon filters and permanent Be and Al windows of the beamline. The measured brightness is close to the calculated value demonstrating that the functioning of the monochromator is well understood. The 10–20% difference may be due to small field errors of the wiggler, which increase the vertical opening of the beam.

The first harmonic reflection Si(222) is very weak, but Si(333) and Si(444) give substantial contributions to the beam. These are separated by the energy-dispersive Ge detector, and their percentage of the total flux is readily estimated. The results are summarized in Fig. 6. It is seen that the harmonic content decreases rapidly with the wiggler field, which is regulated by the magnet gap. Again,

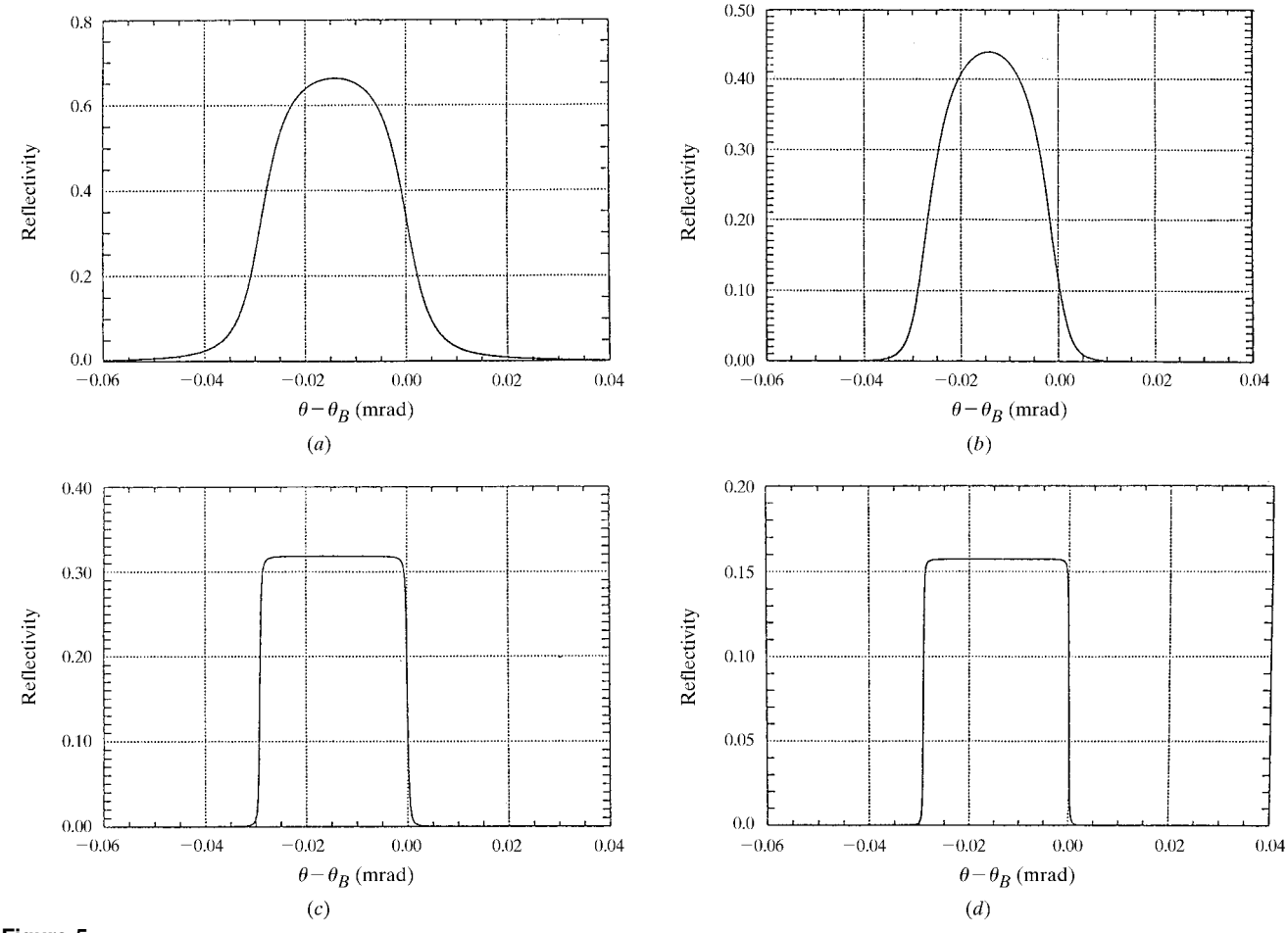

Figure 5
Calculated reflectivity curves for a cylindrically bent Si(*hhh*) crystal. The thickness is 1.2 mm and the angle between the Bragg planes and the surface normal is $\chi = 15°$. The Bragg angle is 4.54°, corresponding to energies of (*a*) 25 keV reflected by Si(111), (*c*) 75 keV by Si(333) and (*d*) 100 keV by Si(444). The combined reflectivity curve $[R(\theta)]^2$ for the fundamental reflection and perfectly matched crystals is shown in (*b*).

Table 1
Calculated central brightness $(d^2F/d\theta d\psi)_o$ of the ID17 wiggler at the minimum gap of 25 mm, integrated reflectivity of the two-crystal Si(*hhh*) monochromator, and monochromatic intensity $n_{o,m,th}$ at fundamental energies of 25 and 33 keV, and at harmonic energies.

The calculated intensity is corrected for absorption in the beamline windows and permanent absorbers by multiplying the brightness by A_{perm}. The experimental intensity $n_{o,m,exp}$ is corrected for attenuation in air and extra absorbers by dividing the Compton scattered flux n_C by A_{exp}.

E (keV)	θ (°)	$(d^2F/d\theta d\psi)_o$ [photons s^{-1} $mrad^{-2}$ $(100\ mA)^{-1}$ $(0.1\%\ bandwidth)^{-1}$]	A_{perm}	Integrated reflectivity (rad)	$n_{o,m,th}$ [photons s^{-1} mm^{-2} $(100\ mA)^{-1}$]	n_C (photons s^{-1})	A_{exp}	$n_{o,m,exp}$ [photons s^{-1} mm^{-2} $(100\ mA)^{-1}$]
25	4.54	1.31×10^{15}	0.657	5.2×10^{-6}	2.51×10^{9}	246	0.323	1.90×10^{9}
33	3.42	1.34×10^{15}	0.772	5.8×10^{-6}	4.46×10^{9}	1009	0.522	4.03×10^{9}
75	4.54	0.90×10^{15}	0.872	1.5×10^{-6}	0.66×10^{9}	222	0.729	0.64×10^{9}
99	3.42	0.60×10^{15}	0.885	0.7×10^{-6}	0.28×10^{9}	43	0.749	0.16×10^{9}

the agreement between calculation and experiment is good, which suggests that calculations can be used for further optimization of the monochromator.

5. Performance tests and imaging results

In addition to measuring the maximum intensity of the beam, the performance of the monochromator was studied with respect to the uniformity and energy distribution of a 120 mm-wide beam. The alignment of the monochromator is complicated, because it is enclosed in an He-filled tank, which has heavy radiation shielding. The bending mechanisms were calibrated by separate measurements at another beamline, and it was verified that the inverse bending radii increased linearly with the actuator travel. At the same time, the approximate zero positions for the tilt drives of the Bragg angles were established. Before closing the monochromator tank the crystals were aligned optically for the setting corresponding to the energy of a *K*-absorption edge, either that of iodine (33.17 keV) or gadolinium (50.24 keV). The crystals were tuned to the non-dispersive position by observing the maximum intensity and then to the absorption edge by coupled motions of θ_1 and θ_2 using I or Gd solutions as absorbers. The detector was an ionization chamber filled with air or nitrogen gas at ambient pressure.

The fine tuning of the monochromator is an iterative procedure, where the goal is to achieve the non-dispersive setting of the two crystals for the whole width and height of the beam. First, the axis of the first crystal must be horizontal, because otherwise there will be a wavelength gradient in the horizontal direction. Second, the axis of the second crystal must be parallel to that of the first one. Third, the bending radii should fulfill the condition of

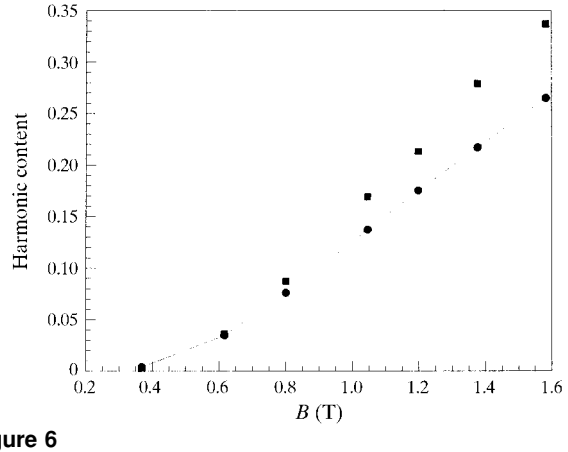

Figure 6
Harmonic content of 75 keV radiation in the 25 keV beam as a function of the wiggler field. The solid line shows the calculated ratio and the squares show the experimental values. Attenuation in the permanent absorbers and beamline windows is included.

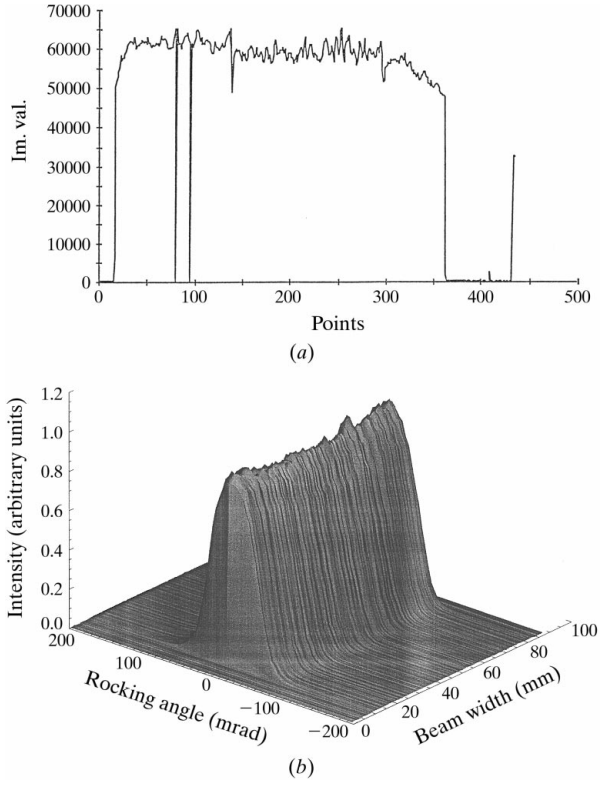

Figure 7
Intensity (Im. val.) and energy distributions of the monochromatic beam at 33 keV. The horizontal distribution of intensity in (*a*) is measured by the 432-element Ge detector with 1.4 ms sampling time, showing effects of noise and bad channels. The pixel width is 0.35 mm. The energy distribution of the beam is analyzed by a perfect Si(511) crystal, and the rocking curve along the crystal is shown in (*b*).

equation (5) to make the virtual line focus of the first crystal the source for the second crystal. Fourth, unequal moments should not be introduced by the bending springs, because this results in a conical shape of the crystal. As the first step, the energy band from the first crystal was analyzed by the second crystal, which was not bent (Suortti *et al.*, 1992). The result was close to the calculated value indicating that there was no energy gradient along the beam. Then the second crystal was bent to the radius given by (5), and the horizontal intensity distribution was recorded (see Fig. 7*a*). It was measured by the main detector of the beamline, a dual Ge detector, which has two horizontal arrays of 432 elements (Elleaume *et al.*, 1999). The two lines are needed in simultaneous recording of the beams bracketing an absorption edge of the contrast agent in subtraction imaging, but in the present case only one

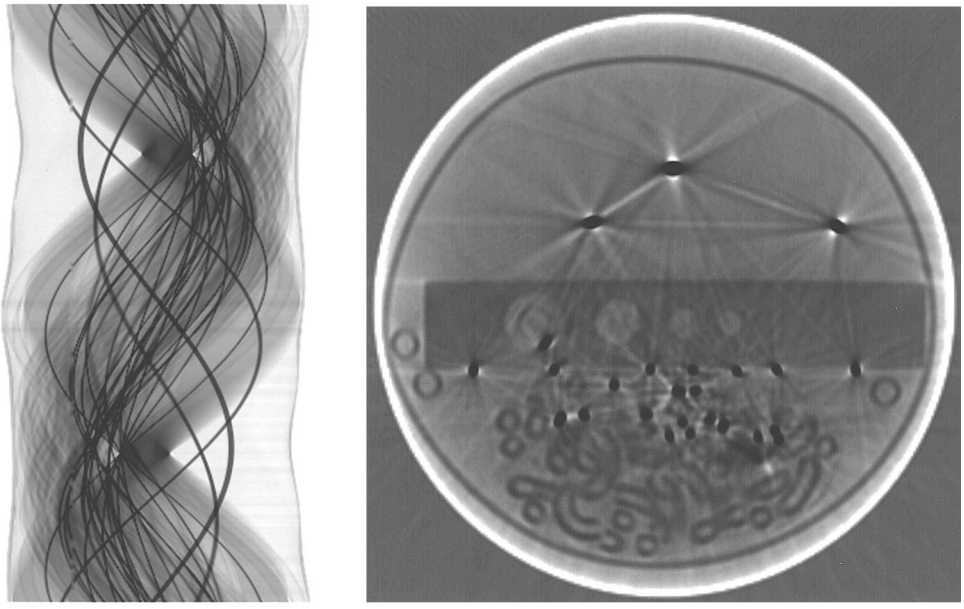

(*a*) (*b*)

Figure 8
Sinogram (*a*) and reconstructed image (*b*) of a phantom containing weakly and strongly absorbing materials taken using 33 keV radiation. The thinnest metal wire is 0.4 mm thick. Starlike artifacts are due to strong contrast variation in the vicinity of thicker wires and needles.

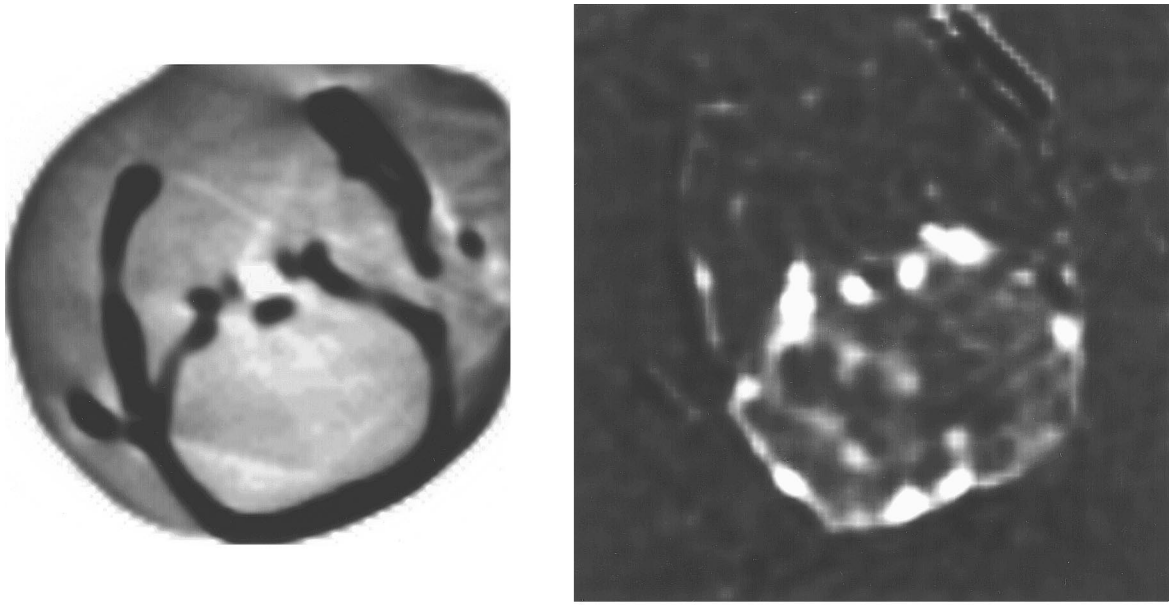

(*a*) (*b*)

Figure 9
Reconstructed *in vivo* image of a rat head taken with 33.5 keV radiation showing the jaws and the contour of the skull (*a*). The distribution of iodine in brain circulation is seen in the temporal subtraction image (*b*). The carotid arteries are seen as bright spots in the middle, and the contour of an implanted tumor in the left part of the skull.

array is used. The sampling time of the detector is short, of the order of 1 ms only. The beam profile is uniform, when the effects of detector noise and bad channels are ignored. Also, an energy analysis of the beam was performed by a flat Bragg-type Si(511) crystal (Fig. 7*b*). The angular width of 65 μrad is due to the vertical energy gradient of the beam, which is convoluted by the bandwidth of each individual ray. It is seen that the mean energy is constant within the 80 mm width of the beam. The long-term stability of the monochromator is excellent, as without any realignment a beam of the same intensity and energy is found before and after a shutdown of several days.

The CT monochromator has been used in the energy range 18–90 keV for studies of phantoms and small animals. A sinogram and reconstructed image are shown in Fig. 8. The transmitted intensity is recorded by the 432-element Ge detector with 2 ms time intervals, which correspond to 0.8° rotation of the phantom. The detector response is normalized by the so-called 'white field' image taken without the phantom. The phantom includes weakly absorbing materials (sponge, macaroni, plastic) and strongly absorbing metal wires and needles to demonstrate the contrast variation and spatial resolution. The resolution appears to be better than the 0.35 mm pixel size of the Ge detector, presumably due to sharing of charge between the neighboring elements and oversampling of projections. Another example is that of reconstructed *in vivo* images of a rat head (Fig. 9). The images were taken in connection with perfusion studies of brain circulation. Iodine contrast solution is injected into the jugular vein, and CT images are taken in rapid succession using 33.5 keV radiation, which is strongly absorbed in iodine. The distribution of iodine is seen in the reconstructed images, when the image taken without iodine is subtracted. A detailed report of this study is in preparation.

6. Summary

The monochromator described in this paper provides a solution to a central problem in computed tomography with synchrotron radiation. A stable monochromatic fixed-exit beam of about 0.1% bandwidth is available at energies between 18 and 90 keV. At the moment the maximum width of the beam is 150 mm. The intensity is sufficient for studies of animals, and experiments with phantoms demonstrate that a human head may be imaged.

The beam is homogeneous in intensity and energy over a horizontal width of 100 mm. However, reaching these conditions requires a time-consuming iterative tuning of the crystals. This can be alleviated by installing beam monitors in the monochromator tank. The Laue-type crystals are not optimized at the moment, because they have the same thickness, and absorption is too large at the low end of the energy range. The height of the thin part of the crystal should be reduced to make cooling more efficient. It is expected that with these improvements the useful width of the beam can be increased to 200 mm or even to 300 mm, which is essential for the ultimate goal of studies of the human head.

.

Help from the engineering and computing staff of the ESRF is gratefully acknowledged. Special thanks are due to Jean-François Adam, Stephanie Corde (CHU), François Esteve (CHU) and Geraldine Le Duc (ESRF), who allowed us to present the *in vivo* images of the rat head prior to publication, and to Marco Di Michiel and Veijo Honkimäki for characterization of the wiggler and calibration of the crystal benders.

References

Dilmanian, F. A. (1992). *Am. J. Physiol. Imaging*, **3/4**, 175–193.
Elleaume, H., Charvet, A. M., Berkvens, P., Berruyer, G., Brochard, T., Dabin, Y., Dominguez, M. C., Draperi, A., Fiedler, S., Goujon, G., Le Duc, G., Mattenet, M., Nemoz, C., Perez, M., Renier, M., Schulze, C., Spanne, P., Suortti, P., Thomlinson, W., Esteve, F., Bertrand, B. & Le Bas, J. F. (1999). *Nucl. Instrum. Methods*, A**428**, 513–527.
Elleaume, H., Charvet, A. M. & Le Bas, J. F. (1997). *Acta Radiol. Suppl.* **38**(412), 29–41.
Graeff, W. & Engelke, K. (1991). *Handbook of Synchrotron Radiation*, Vol. 4, pp. 361–405. Amsterdam: North-Holland.
Illing, G., Heuer, J., Reime, B., Lohmann, M., Menk, R. H., Schildwächter, L., Dix, W.-R. & Graeff, W. (1995). *Rev. Sci. Instrum.* **66**, 1379–1381.
Kato, N. (1964). *J. Phys. Soc. Jpn*, **19**, 971–985.
Nagata, Y., Yamaji, H., Hayashi, K., Kawashima, K., Hyodo, K., Kawata, H. & Ando, M. (1992). *Rev. Sci. Instrum.* **63**, 615–618.
Penning, P. & Polder, D. (1961). *Philips Res. Rep.* p. 419.
Ren, B., Dilmanian, F. A., Chapman, L. D., Ivanov, I., Wu, X. Y., Zhong, Z. & Huang, X. (1999). *Nucl. Instrum. Methods*, A**428**, 528–550.
Schulze, C. & Chapman, D. (1995). *Rev. Sci. Instrum.* **66**, 2220–2223.
Schulze, C., Lienert, U., Hanfland, M., Lorenzen, M. & Zontone, F. (1998). *J. Synchrotron Rad.* **5**, 77–81.
Schulze, C., Suortti, P. & Chapman, D. (1994). *Synchrotron Rad. News*, **7**(3), 8–11.
Suortti, P., Chapman, D., Schneider, J. R. & Tschentscher, T. (1992). *J. Appl. Cryst.* **25**, 432–438.
Suortti, P., Lienert, U. & Schulze, C. (1997). *AIP Conf. Proc.* **389**, 175–192.
Suortti, P. & Thomlinson, W. (1988). *Nucl. Instrum. Methods*, A**269**, 639–648.
Suortti, P., Thomlinson, W., Chapman, D., Gmür, N., Siddons, D. P. & Schulze, C. (1993). *Nucl. Instrum. Methods*, A**336**, 304–309.
Thomlinson, W. (1996). *Proceedings of the International School of Physics 'Enrico Fermi'*, Course CXXVIII, edited by E. Burattini & A. Balerna, pp. 127–153. Amsterdam: IOS Press.
Thompson, A. C., Llacer, J., Campbell Finman, L. C., Hughes, E. B., Otis, J. N., Wilson, S. & Zeman, H. D. (1984). *Nucl. Instrum. Methods*, **222**, 319–323.